iScience

CellPress
OPEN ACCESS

Review

Aggregation-induced emission luminescence for angiography and atherosclerotic diagnosis

Yuxun Ding,[1] Guanchu Ou,[1] and Dong Wang[1,*]

SUMMARY

Optical imaging technology has become increasingly recognized for its utility in diagnosing atherosclerosis thanks to advantages such as high spatial resolution, rapid data acquisition, lack of radiation exposure, cost-effectiveness, minimal invasiveness, and limited side effects. However, traditional luminogens employed in optical diagnostics are often troubled by aggregation-caused quenching (ACQ) effect, causing diagnostic errors *in vivo*. Since Professor Tang discovered the aggregation-induced emission (AIE) phenomenon, AIE luminogens (AIEgens) have been rapidly developing and are considered as the next-generation fluorescent contrast agents for angiography and atherosclerotic diagnosis. This mini review will outline the use of AIEgens in angiography and the diagnosis of atherosclerosis, exploring different imaging models, including second near-infrared, two/multi-photon, and photoacoustic imaging, and will provide a forward-looking perspective on their potential in atherosclerotic diagnosis.

INTRODUCTION

Cardiovascular disease (CVD) is the primary cause of death globally, affecting over 523 million people globally.[1] Atherosclerosis, a chronic disease involving the arterial wall, is a major contributor to CVD.[2] Therefore, early diagnosis and treatment of atherosclerosis are crucial for preventing CVD.[2] Clinically, atherosclerosis can be diagnosed using various imaging techniques, including computed tomography (CT),[3] magnetic resonance imaging (MRI),[4] positron emission tomography (PET),[5] and single-photon emission computed tomography (SPECT).[6] However, these technologies have significant drawbacks, including high costs; the ionizing radiation associated with CT, PET, and SPECT; and the limited spatial resolutions of MRI and PET.

In contrast, the optical imaging offers numerous advantages in disease diagnosis, such as high spatial resolution, rapid data acquisition, absence of radiation risks, cost-effectiveness, minimal invasiveness, and limited side effects.[7] Thereby, optical imaging is considered as one of the most promising candidates for the next generation of diagnostic technology. The principle of optical imaging is based on luminogens, which can absorb light, sound, or chemical energy and convert it into detectable fluorescence.[8] Commonly used luminogens includes Cyanine5 (Cy5), Cyanine7 (Cy7), and indocyanine green (ICG).[9] However, these luminogens typically experience reduced fluorescence emission at high concentrations or in aggregated states due to the aggregation-caused quenching (ACQ) effect, indicating a less suitable sensing approach for practical use in atherosclerosis diagnosis.[10]

In this case, anti-ACQ luminogens, known as aggregation-induced emission (AIE) luminogens (AIEgens), have served as a new kind of organic light-emitting material, showing advantages in strong emission in an aggregation state, large Stokes shifts, and high photobleaching thresholds.[11–14] Unlike ACQ luminogens, AIEgens display minimal or low emission in solution, yet exhibit strong fluorescence in aggregated form.[15] In aggregate state, limiting intramolecular motion may enhance radiative decay, thus enhancing fluorescence emission intensity.[16] Since Professor Tang proposed the concept of AIE in 2001, various AIEgens with distinct excitation and emission wavelengths have been developed and utilized in bioimaging and disease diagnosis.[17] Notably, recent advancements in AIEgens featuring second near-infrared (NIR-II) emission, two-photon or multi-photon imaging, and photoacoustic imaging (PAI) significantly enhance tissue fluorescence penetration depth *in vivo*.[18–20] These AIEgens effectively address the critical limitation of inadequate tissue penetration associated with traditional optical imaging techniques.[21] In particular, the development of nanotechnology can effectively improve the targeting efficiency of small molecules,[22–28] promoting the wide used of AIEgens in the angiography and atherosclerotic diagnosis.

In this mini review, we seek to investigate the use of AIEgens in diagnosing and treating atherosclerosis. We will discuss AIEgens from various imaging modalities, including fluorescence imaging, NIR-II imaging, two-photon or multi-photon imaging, and PAI, focusing on their application in atherosclerosis diagnosis. Then, we will detail the challenges associated with using AIEgens in the diagnosis of atherosclerosis. This review aims to offer perspectives on the possibilities of AIEgens within this field and encourage further research on this promising topic (Figure 1).

[1]Center for AIE Research, College of Materials Science and Engineering, Shenzhen University, Shenzhen 518060, China
*Correspondence: wangd@szu.edu.cn
https://doi.org/10.1016/j.isci.2024.110719

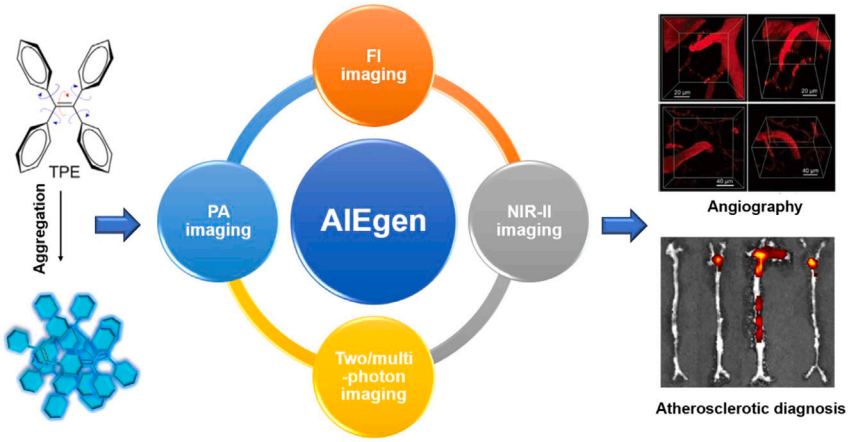

Figure 1. Illustration for the application of AIEgens in angiography and atherosclerotic diagnosis

ACQ AND AIE

ACQ is a phenomenon widely recognized in organic fluorescent dyes and generally regarded as unfavorable for bioimaging.[29] For instance, fluorescein isothiocyanate (FITC) exhibits strong green fluorescence in a monomolecular state when fully dissolved in water. However, its fluorescence intensity diminishes an increasing concentration of acetone in a water/acetone mixture. When the acetone proportion exceeds 80%, the fluorescence is almost completely quenched.[30,31] Since organic molecules naturally aggregate in biological media, the ACQ effect compels researchers to use very dilute fluorescent probes, making them more susceptible to photobleaching.[29] This effect directly leads to the difficulty of using ACQ molecules in aqueous biological environments.[32,33]

Conversely, tetraphenylethylene (TPE), a typical AIE molecule, exhibits almost no emission when fully dissolved in tetrahydrofuran (THF) but emits intense blue fluorescence in a THF/water mixture with increasing water content (Figure 2A).[34,35] The AIE mechanism has been fundamentally attributed to the limitation of intramolecular motion, encompassing limitation of intramolecular rotation and vibration (Figure 2B).[36] Taking advantage of the AIE effect, AIEgens have emerged as a class of fluorescence probes exclusively used within biological organisms and are extensively used in biological imaging and disease diagnosis, such as CVD and cancer diagnosis.[37–39]

AIEgens FOR ANGIOGRAPHY AND ATHEROSCLEROTIC DIAGNOSIS

AIEgens for atherosclerosis fluorescence imaging

The visible and near-infrared imaging

Thanks to their superior fluorescence imaging capabilities, AIEgens have been extensively utilized in disease diagnosis. However, initially developed AIEgens emitted at short emission wavelengths, mainly in the visible (400–700 nm) and near-infrared (700–1,000 nm) ranges, making them impossible to directly diagnose diseases *in vivo*. Therefore, early diagnostics using AIEgens predominantly relied on *ex vivo* fluorescence imaging.

For instance, Liu et al. created a reactive oxygen species (ROS)-responsive targeted fluorescent nanoprobe using AIEgen, named TPAM, for detecting atherosclerotic plaques. In this design, TPAM was conjugated to maleimide (polyethylene glycol) hydroxyl through an ROS-responsive cleavable bond and later functionalized with CLIKKPF peptide to target foam cells in atherosclerotic plaques specifically (Figure 3A).[40] The fluorescence from TPAM enabled clear observation of the plaques in *ex vivo* aortas (Figure 3B). Especially, with the help of CLIKKPF peptide, TPAM can more efficiently accumulate in plaque (Figure 3C), thus enhancing diagnostic accuracy for atherosclerosis. Similarly, Wang et al. engineered an ROS-responsive prodrug copolymer (PMPC-P(MEMA-co-PDMA)), and it was co-loaded with an AIEgen, namely LFP, into a red blood cell membrane to self-assemble surface-biomimetic nanoparticles (RBC/LFP@PMMP) (Figure 3D).[41] With ROS responsiveness, RBC/LFP@PMMP can be interrupted and achieved targeted release of LFP at inflammatory atherosclerotic tissue for atherosclerosis theranostics (Figures 3E and 3F).

Employing the same strategy, various nanoprobes based on AIEgens have been developed for *ex vivo* atherosclerotic diagnosis. For example, Zhang et al. designed two AIEgens, TTM and MeO-TTM, using malononitrile as the electron acceptor and triphenylamine or 4-methoxy triphenylamine as the electron donors. The introduction of the methoxy group caused the emission wavelength of MeO-TTM to redshift from 575 nm to 660 nm, enabling clear bioimaging of atherosclerosis.[42] To enhance the targeting efficiency of AIEgens, He et al. developed an ROS-responsive and CD44-targeted nanoplatform for the targeted delivery of AIEgens, leveraging the high ROS levels and CD44 receptor expression in the atherosclerotic microenvironment. This dual-targeting nanoplatform enables AIEgens to effectively accumulate in atherosclerotic plaques, providing a precise diagnostic technology for atherosclerosis diagnosis.[43] Using a similar strategy, Xu et al. constructed a multifunctional nanoparticle (LFP/PCDPD) with active targeting capabilities. This targeting is achieved through the high affinity of dextran to the vascular adhesion molecule-1 (VCAM-1) and the CD44 receptor on the surface of damaged endothelial cells,

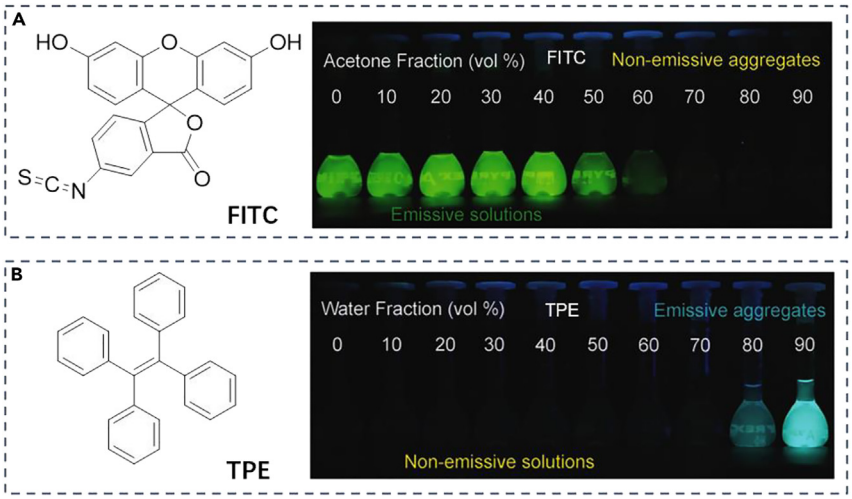

Figure 2. The representative ACQ and AIE molecule

(A and B) The structure and fluorescence photographs of FITC (A) and TPE (B), typical ACQ and AIE luminogens, respectively, in solution or suspension in water/acetone mixtures with different acetone fractions and in THF/water mixtures with different water fractions. Reproduced with permission from Feng et al.[35] Copyright 2016 WILEY-VCH.

as well as the elevated ROS levels in atherosclerotic plaques.[44] These findings highlight the significant benefits of AIEgens in diagnosing atherosclerosis.

The NIR-II imaging

To address the issue of insufficient tissue penetration by visible and NIR-I light, the NIR-II (1,000–1,700 nm) emissive AIEgens were progressively developed following Liu et al.'s first documentation of an AIEgen exhibiting NIR-II emission in 2018.[10,45] Compared to visible or NIR-I imaging, NIR-II imaging greatly diminishes background noise and improves tissue penetration depth (5–20 mm) because of reduced photon scattering and minimal tissue absorption.[10,46,47] According to the emission wavelength, NIR-II imaging can be further classified into NIR-IIa (1,000–1,500 nm) and NIR-IIb (>1,500 nm). Both categories are applicable for *in vivo* vessel imaging and diagnosing atherosclerosis.

The quality of NIR-II imaging primarily depends on two key factors: long emission wavelength and high fluorescence quantum yield (QY).[10] In molecular design, expanding π-conjugation length and enhancing electron donors and acceptors (D-A) strength can both reduce the highest occupied orbital (HOMO)-lowest empty orbital (LUMO) gap, leading to a red-shifted emission. However, due to the small molecular weight of AIEgens, expanding the π-conjugation length has minimal effect on extending their emission wavelength. A promising alternative is to introduce substituents with electron donors (D) and acceptors (A), as electron donors can elevate the HOMO level and electron acceptors can lower the LUMO level. The strategy of enhancing electron D-A strength has been widely employed in the design of NIR-II AIEgens. According to the energy gap theory, the QY decreases with the redshift of emission wavelength into the NIR region due to vibrational overlap of ground and excited states, severely compromising the imaging capability of AIEgens. Researchers analyzing the energy level diagram found that QY is inversely related to heat and the twisted intramolecular charge transfer (TICT) process.[48] To improve QY, Hong et al. reported a strategy to efficiently suppress the TICT process of AIEgens,[49] while Tang et al. increased radiative decay by preventing close intermolecular interactions. These methods effectively enhance the QY of AIEgens, thereby promoting the application of near-infrared imaging in disease diagnosis and treatment.

The NIR-IIa imaging. After extensive research, various AIEgens have been developed for NIR-II imaging. Qin et al. created supramolecular cages with AIE characteristics using D-A-D adducts as the fundamental building blocks. By enhancing the electron-attracting ability through the replacement of central electron acceptors, the optical band gap was effectively narrowed, shifting the fluorescence emission from the red region (606 nm) to the NIR-II region (986 nm) (Figures 4A–4C). *In vivo* studies demonstrated that the brain vasculature in mice could be clearly observed through an unopened scalp and skull, indicating potential applications in monitoring cerebrovascular diseases (Figures 4D and 4E).[50] This strategy provides a convenient and efficient method for creating NIR-II supramolecular cages for disease diagnosis, particularly for cerebrovascular diseases.

Using molecular engineering techniques, Xu et al. developed a D–π-A–π-D-type NIR-II AIEgen, named AX1. Due to their intrinsic AIE enhancement properties, these AIEgens exhibit a high fluorescence QY of 14.8%, allowing for high-resolution imaging of blood vessels *in vivo*.[51] To improve bioavailability and biosafety *in vivo*, Gao et al. utilized endogenous albumin as an efficient carrier to encapsulate AIEgens (TT), forming an albumin-AIEgen nanoparticle named B-TT. This albumin-consolidated strategy effectively inhibited the intramolecular vibrations of AIEgens, thereby increasing the fluorescence QY and achieving high-resolution cerebrovascular imaging with a high signal-to-background ratio (SBR, ~90) in mouse models.[52] These developments demonstrate that AIEgens with highly emissive fluorescence in the NIR-II window may offer an alternative approach for vascular disease diagnosis.

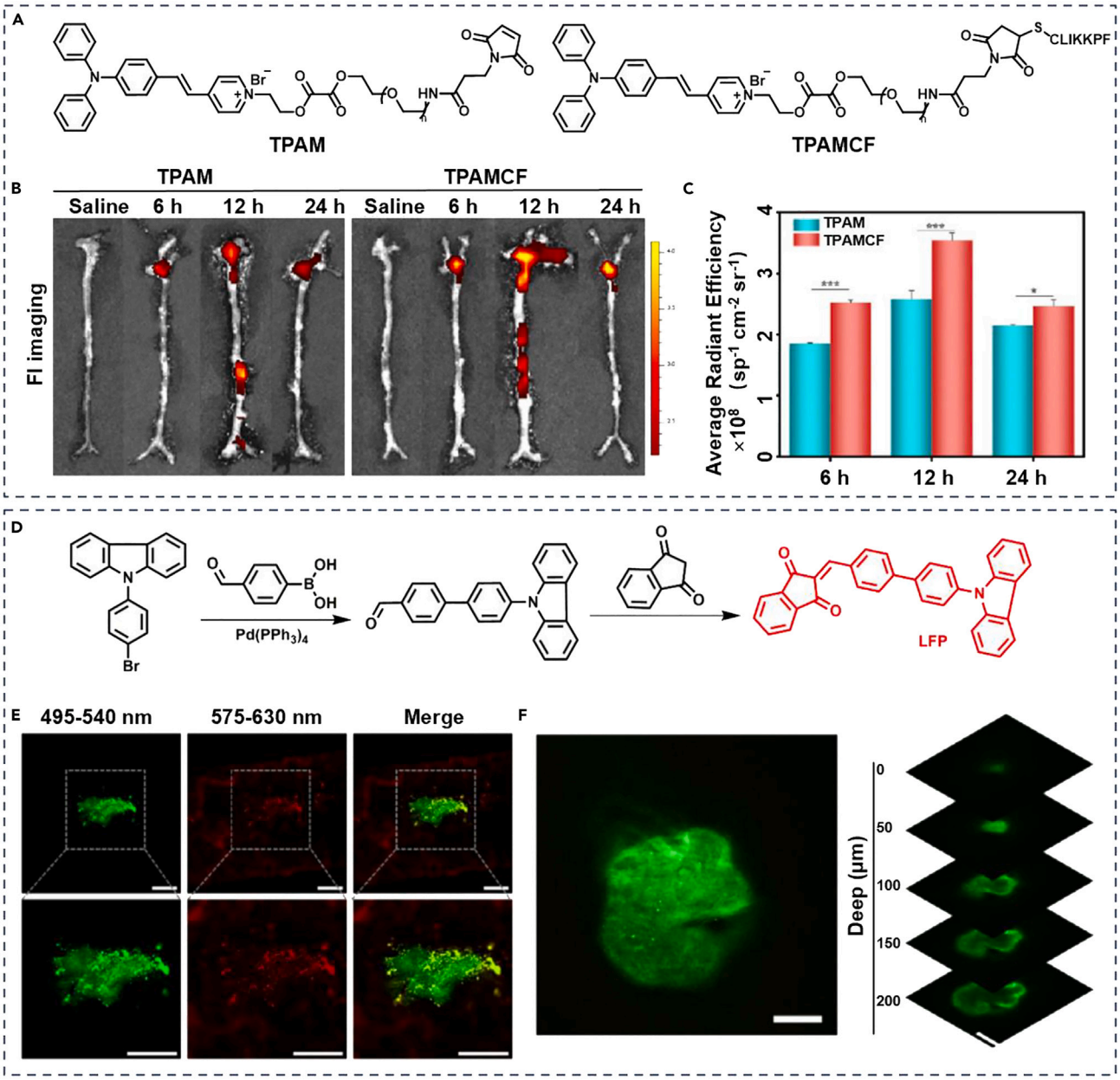

Figure 3. AIEgens for *ex vivo* atherosclerosis diagnosis via fluorescence imaging

(A) The structure of TPAM and TPAMCF.

(B and C) Representative fluorescence images and quantitative analyses of the aorta isolated from ApoE$^{-/-}$ mice, sacrificed at 6, 12, or 24 h post intravenous injection of saline, TPAM nanoperticles (NPs), or TPAMCF NPs. Reproduced with permission from Liu et al.[40] Copyright 2023 American Chemical Society.

(D) Synthesis route of LFP.

(E and F) Confocal images of *en face* LFP-stained aortas and plaques at various imaging depths. Reproduced with permission from Ma et al.[41] Copyright 2021 American Chemical Society.

The NIR-IIb imaging. To further enhance tissue penetration in NIR-II imaging, numerous AIEgens with excitation wavelengths exceeding 1,500 nm have been developed for vascular imaging and related disease diagnosis.[53] Li et al. designed a novel benzo-bis(1,2,5-thiadiazole)-based AIEgen (HY4) (Figure 5A), characterized by NIR-IIb emission and remarkably high fluorescence QY as high as 14.45% in the NIR-II region. To improve its biocompatibility, HY4 was loaded into a lipid nanoparticle using self-assembly technology. These nanoparticles exhibited a hydrodynamic diameter of approximately 100 nm and fluorescence intensity approximately 7.5 and 6 times greater than those of ICG and IR-26, respectively. Thus, HY4 nanoparticles facilitate high-quality fluorescence imaging under a 1,500 nm photoluminescence (PL) filter.[54]

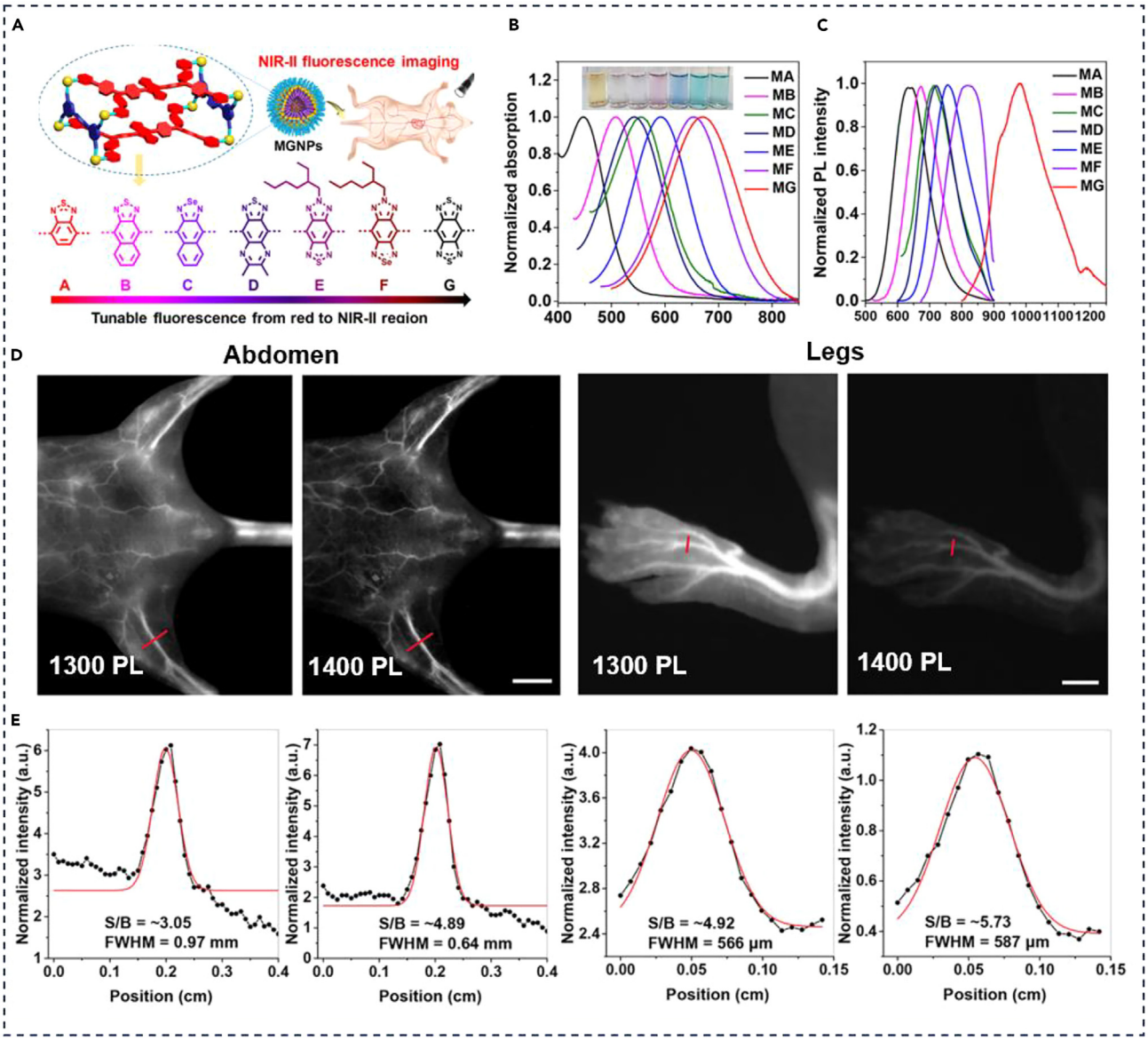

Figure 4. AIEgens for the NIR-IIa imaging of vessel

(A) Schematic illustration of the fluorescence regulation strategy from red to NIR-II region by turning the acceptor.

(B and C) Normalized absorption and emission spectra of cages MA-MG.

(D and E) The NIR-II imaging at hindlimb and paw under different LP filters (1,300 nm and 1,400 nm) and the corresponding fluorescence intensity profiles of the highlighted blood vessels with red lines. Reproduced with permission from Qin et al.[50] Copyright 2023 American Chemical Society.

Similarly, Tang at al. suggested a molecular design approach for NIR-IIb AIEgens by controlling the effects of TICT and successfully developed an NIR-IIb AIE probe with QY of 11.5% in the NIR-II region and a longer mission up to 1,600 nm. This probe was used for NIR-IIb fluorescence imaging in the cerebral vasculature of BALB/c nude mice, achieving high-performance angiography with sharp resolution and high SBR, thereby demonstrating significant advantages for *in vivo* imaging.[55] Owing to these advancements, a multitude of NIR-IIb probes have been developed over the past decade[56,57] and applied in bioimaging and disease diagnosis.

AIEgens for atherosclerosis two/multi-photon imaging

Two-photon excitation fluorescence (2PEF) is defined as the phenomenon where two photons arrive simultaneously within an attosecond (10^{-18} s) time window and jointly excite a fluorophore.[58] Therefore, the use of photon pairs with different energies whose combined energy matches the energy gap between S0 and S2 can achieve this process.[59,60] Compared to traditional single-photon fluorescence imaging, 2PEF

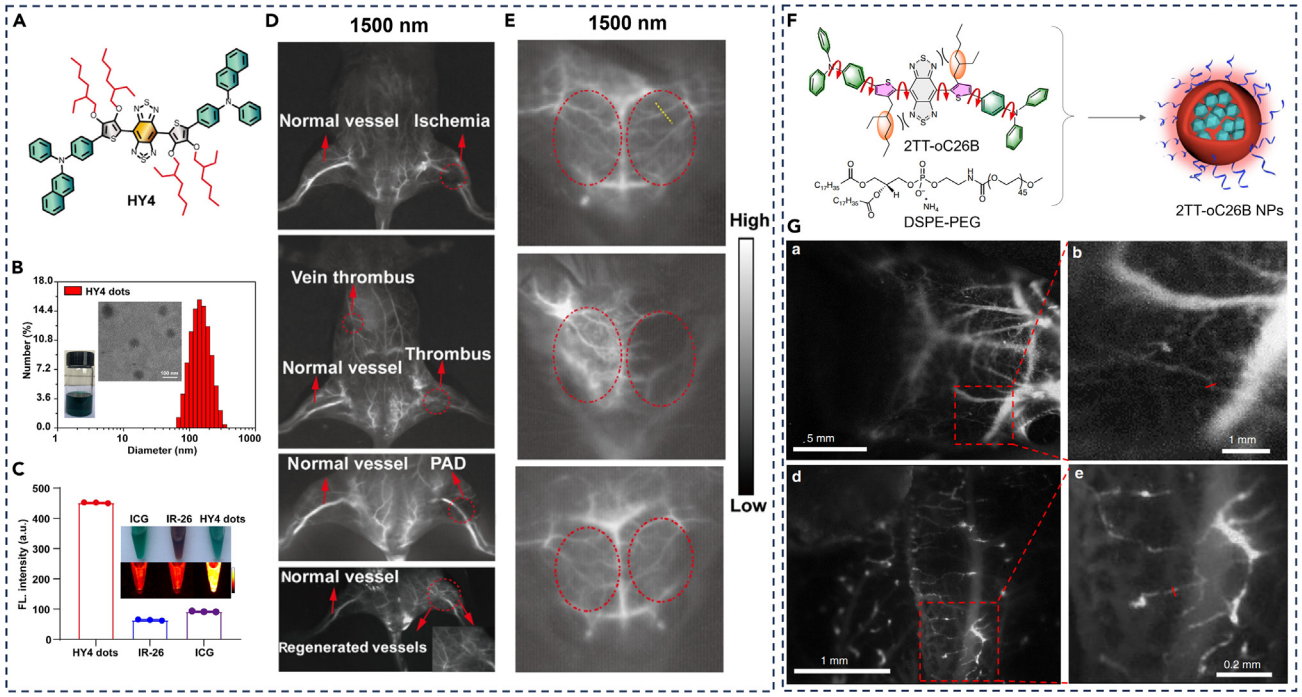

Figure 5. AIEgens for the NIR-IIb imaging of vessel

(A) The chemical structures of HY4.

(B) The TEM and dynamic light scattering (DLS) images of HY4 dots, scale bar, 100 nm.

(C) The fluorescent intensity of IR-26 in DCE, ICG in water, HY4 dots in aqueous solution with the concentration.

(D) *In vivo* NIR-IIb fluorescence imaging after ligation of femoral artery and vein (red dotted circles region).

(E) *In vivo* NIR-IIb imaging for ischemic stroke. Reproduced with permission from Li et al.[54] Copyright 2022 Chinese Chemical Society.

(F) Schematic illustration of 2TT-oC26B NPs.

(G) NIR-IIb fluorescence image using a 50 mm fixed focal lens and a scan lens (Thorlabs). Reproduced with permission from Li et al.[55] Copyright 2020 Springer Nature.

imaging is particularly beneficial for deep tissue imaging.[61] Additionally, 2PEF imaging benefits from a more efficient light collection pathway than that found in single-photon confocal microscopy.[62]

Taking advantage of the deep penetration capabilities of 2PEF, certain AIEgens have been modified through molecular engineering to achieve two-photon imaging for atherosclerosis imaging.[63] For example, Bo et al. developed a smart probe with AIE property, namely IND, for concurrent dual-color imaging of atherosclerotic plaques (Figure 6A).[64] Leveraging its high lipid specificity, deep tissue penetration, and excellent two-photon imaging capabilities, IND enables high-resolution imaging for detailed mapping of three-dimensional lipid distributions in mouse atherosclerotic plaques. Using two-photon imaging, the researchers observed that lipids within the plaques are morphologically diverse, exhibiting various shapes and sizes. The lipid quantity at four different plaque depths is positively correlated with the plaque area. The size of lipid regions typically ranges from 0.1 mm^2 to 30 mm^2, with the largest lipid accumulation area being 241.6 mm^2, located at a depth of 15 mm (Figure 6B).[64] In response to the high levels of ROS present in the inflammatory microenvironment of atherosclerosis, Ma et al. utilized an ROS-responsive bond to attach an AIEgen (TP) with 2PEF imaging capabilities to prednisolone (Pred), a widely used anti-inflammatory drug. Subsequently, the compound, referred to as TPP, was encapsulated within core-shell structured micelles (TPP@PMM) through self-assembly using the amphipathic polymer (Figure 6C).[65] When entering atherosclerotic plaque, the ROS-responsive bond breaks to release the TPP (Figure 6D) and thus could be distinctly visualized on the *en face* of the aortas using 2PEF (Figures 6E and 6F). Importantly, this design simultaneously facilitates targeted inflammation therapy for atherosclerosis. As TPP@PMM accumulates at the atherosclerotic site, an ROS-triggered conversion from hydrophobic to hydrophilic occurs in PMEMA for releasing TPP. Subsequently, the ROS-responsive bond in TPP is cleaved for the targeted delivery of Pred, enabling precise, two-photon imaging-guided therapy for atherosclerosis.[65]

Similar with 2PEF, three-photon excitation fluorescence (3PEF) describes the phenomenon where three photons simultaneously arrive within an attosecond time window and collectively excite a fluorophore. However, 3PEF achieves deeper tissue penetration compared to 2PEF.[66,67] Recently, specific AIEgens have been specifically developed for CVD bioimaging applications.[68,69] For example, Xu et al. synthesized three type of AIEgens, including TPA-BT, DPNA-BT, and DPNA-NZ (Figure 7A), for the three-proton imaging of blood vessel of the brain. By enhancing D-A strength of N,N-diphenylnaphthalen-1-amine (DPNA) and naphtho[2,3-c]-[1,2,5]thiadiazole (NZ), the average fluorescence emission wavelength of DPNA-NZ was extended to 702 nm, with the maximal absorption wavelength at 533 nm (Figures 7B and 7C).

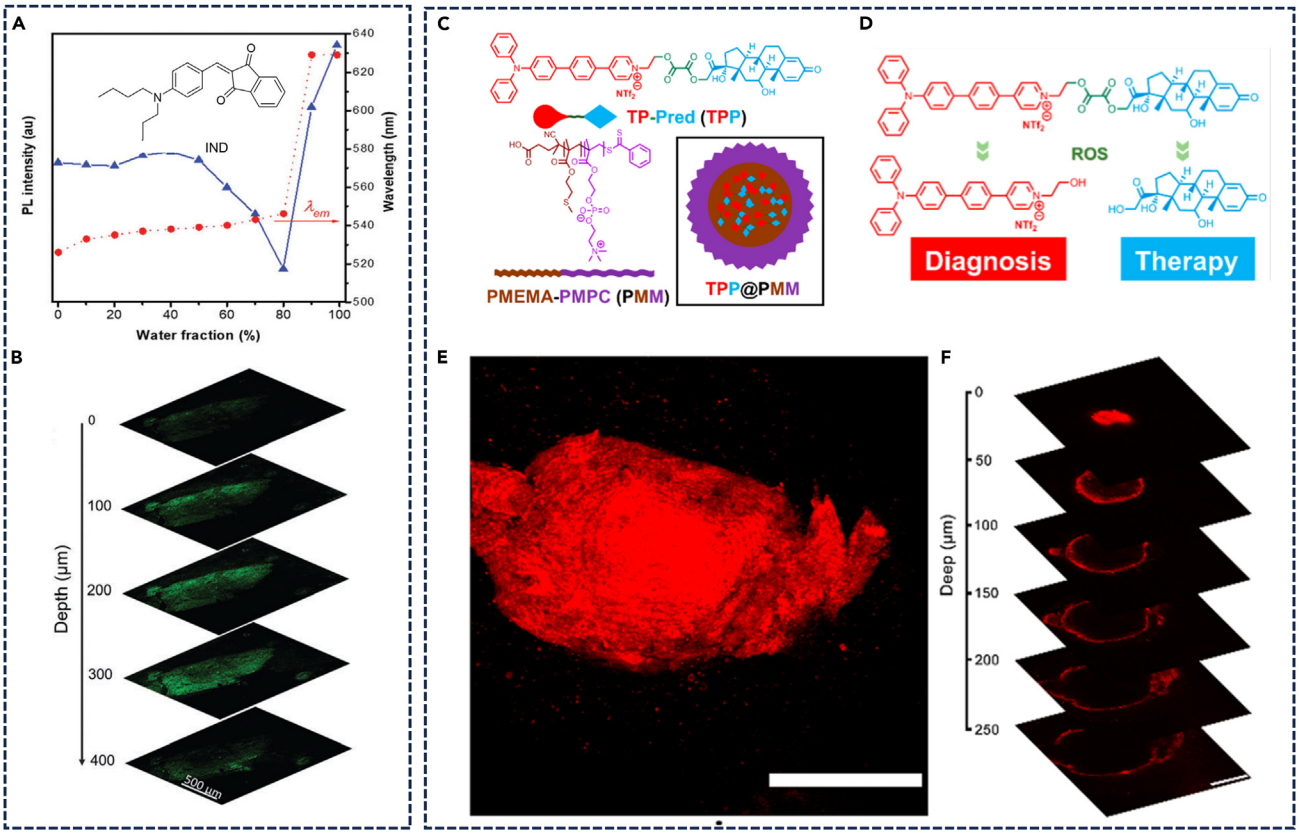

Figure 6. AIEgens with 2PEF capabilities for atherosclerosis two-photon imaging

(A) The structure and AIE characteristic of IND versus the composition of THF/water mixtures with various water fractions.

(B) Two-photon images of IND in atherosclerotic plaques at various imaging depths. Reproduced with permission from Situ et al.[64] Copyright 2019 Royal Society of Chemistry.

(C) The self-assembly of TPP@PMM.

(D) ROS-responsive process of TPP@PMM.

(E) Two-photon image of TPP@PMM in atherosclerotic plaques.

(F) Two-photon images of TPP@PMM in plaques at various imaging depths. Reproduced with permission from Ma et al.[65] Copyright 2020 American Chemical Society.

For *in vivo* imaging, DPNA-NZ was loaded with distearoyl phosphatidyl ethanolamine - polyethylene glycol (DSPE-PEG) to form DPNA-NZ nanoperticles (NP). The absorption and emission spectra of these AIEgen NPs were similar to those of single molecule (Figure 7D). By *In vivo* imaging, the vasculature and microvessel in deep mouse brain were clearly visualized using DPNA-NZ NPs as the contrast agent (Figure 7E).[68] Similarly, Wang et al. employed TPAPhCN dots, a specific type of AIEgen with 3PEF properties, to detect atherosclerotic plaques in the brain vasculature and carotid arteries (Figures 7F and 7G).[70] In addition, Zhu et al. designed a photostable luminogen with AIE properties, identified as TPE-TPP, which utilizes femtosecond laser excitation at 1,020 nm for three-photon imaging in *ex vivo* brain tissue.[71] To further expand the application of AIEgen with 3PEF, Qiu et al. synthesized an AIEgen with ultrabright far-red/near-infrared emission, namely BTF, which can facilitate *in vivo* three-photon imaging of brain vasculature through the intact skull.[72] Benefiting from the deep penetration capabilities of three-photon imaging, these luminogens have been applied to atherosclerosis diagnosis. Utilizing a three-photon microscope, the researchers not only identified atherosclerotic plaques but also enabled efficient *in vivo* labeling and imaging of lipids in deep tissues.

AIEgen for atherosclerosis PAI imaging

PAI is an emerging technology with significant potential for both preclinical biomedical research and clinical applications.[73] This technique utilizes the absorption of intensity-modulated light by tissues to produce broadband acoustic waves. The local absorption leads to minor heating, which induces rapid thermoelastic expansion that generates photoacoustic waves.[74] Consequently, photoacoustic (PA) imaging combines the robust optical contrast of light with the high spatial resolution characteristics of ultrasound.[75]

Recent research indicates that PAI can be effectively applied in atherosclerosis imaging. For example, Xu et al. developed a novel photoacoustic contrast agent, a π-conjugated polymer (PMeTPP-MBT), which was then incorporated into a VCAM-1- and CD44-targeted nanoparticle, named PA/ASePSD. This nanoparticle facilitates accurate photoacoustic diagnosis *in vivo* and shows promise as a

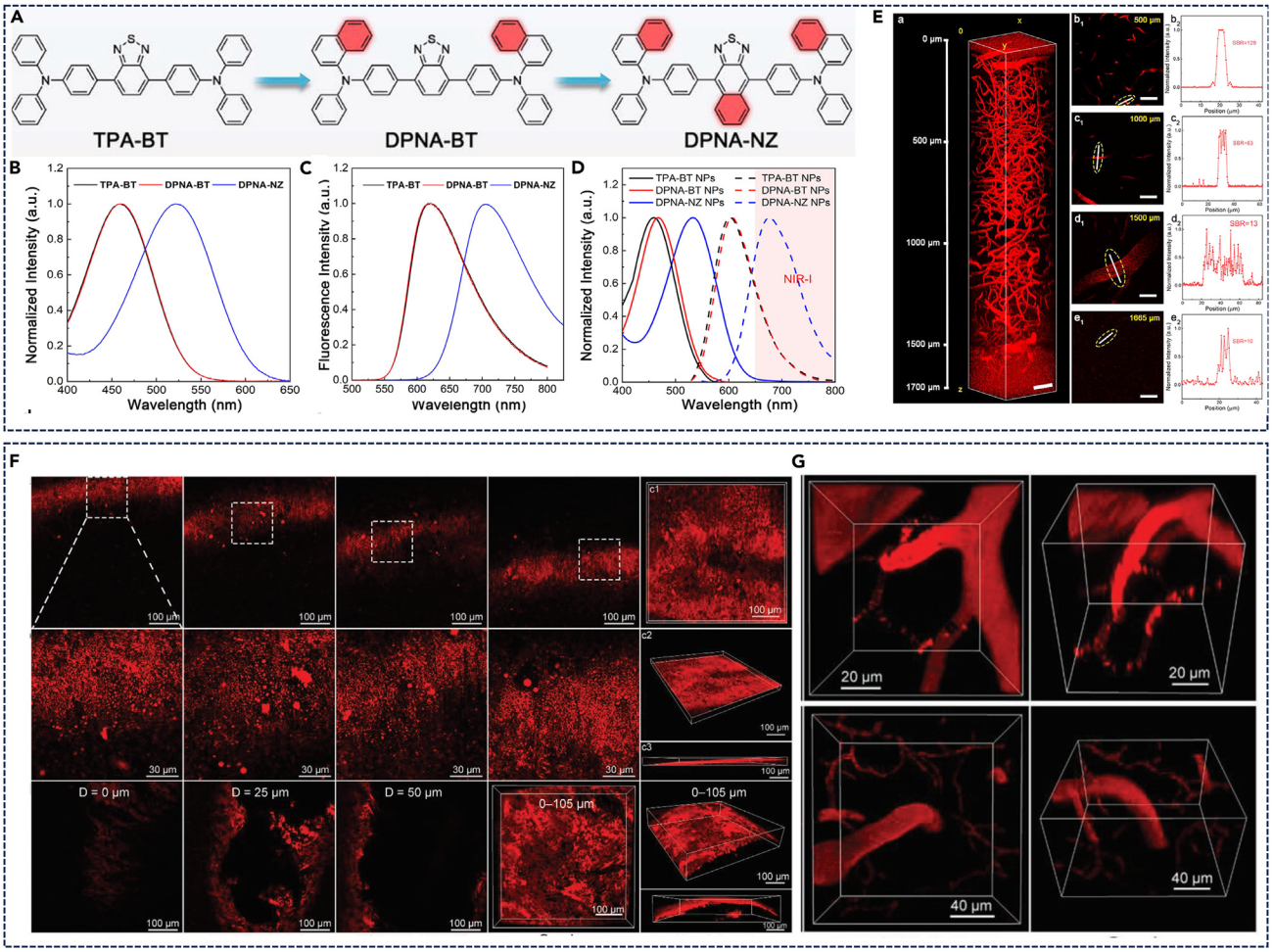

Figure 7. AIEgens with 3PEF capabilities for atherosclerosis three-photon imaging

(A) Molecular design of 3P AIEgens, including TPA-BT, DPNA-BT, and DPNA-NZ.

(B and C) The absorption spectra of AIEgens in THF and fluorescence spectra of AIEgens in the solid state.

(D) Normalized absorption and emission spectra of AIEgen NPs in water (solid line: absorption, dashed line: emission).

(E) 2D and 3D reconstructed images of brain vasculature by DPNA-NZ NPs. Scale bar: 100 μm. Reproduced with permission from Xu et al.[68] Copyright 2020 American Chemical Society.

(F) Intravital 3PEF images, enlarged 3PEF images and 3D reconstructed 3PEF images of TPAPhCN-dots-labeled atherosclerotic plaques on the carotid artery vessel wall at different depths.

(G) 3D reconstructed 3PEF images of TPAPhCN-dots-labeled atherosclerotic plaques on the brain blood vessel wall and normal brain blood vessels. Reproduced with permission from Wang et al.[70] Copyright 2021 WILEY-VCH.

candidate for early-stage atherosclerosis theranostics (Figure 8A).[76] Similarly, Xie et al. developed a molecular probe (PBD-CD36) with PAI capabilities to specifically target CD36 overexpressed in atherosclerotic plaques for the diagnosis of atherosclerosis (Figure 8B).[77] Additionally, Ma et al. constructed a theranostic nanoplatform to incorporate a polymeric photoacoustic probe into nanoparticles designated as PLCDP@PMH, for noninvasive *in vivo* diagnosis of atherosclerosis.[78] Ge et al. introduced an advanced nanoprobe with improved PAI property for direct, noninvasive *in vivo* imaging for the diagnosis of atherosclerosis.[79] Mahsa Gifani's team crafted a special targeted nanoparticle with PAI capabilities for targeting inflammatory Ly-6Chi, a type of abundant immune cell in the arterial wall, accurately identifying and diagnosing inflamed atherosclerotic lesions.[80] Qin et al. designed a gold nanorod conjugated with MMP2 antibody (AuNRs-Ab) for targeting the expression of MMP_2 in the atherosclerotic plaques, thereby enabling highly efficient PAI diagnostics for atherosclerosis.[81]

These studies collectively confirm that PAI is an excellent detection technology for atherosclerosis diagnosis. Although there are no reports of AIEgens being used in the PAI of atherosclerosis, AIEgen is still a very potential contrast agent of PAI, as evidenced in other diseases.[83] For example, Sheng et al. designed a new NIR-II AIEgen for the PAI of brain tumor (Figure 8C). After injection, PA signals in the brain tumor gradually increased over time (Figure 8D), indicating that this AIEgen can be employed for the precise diagnosis of brain cancer via its

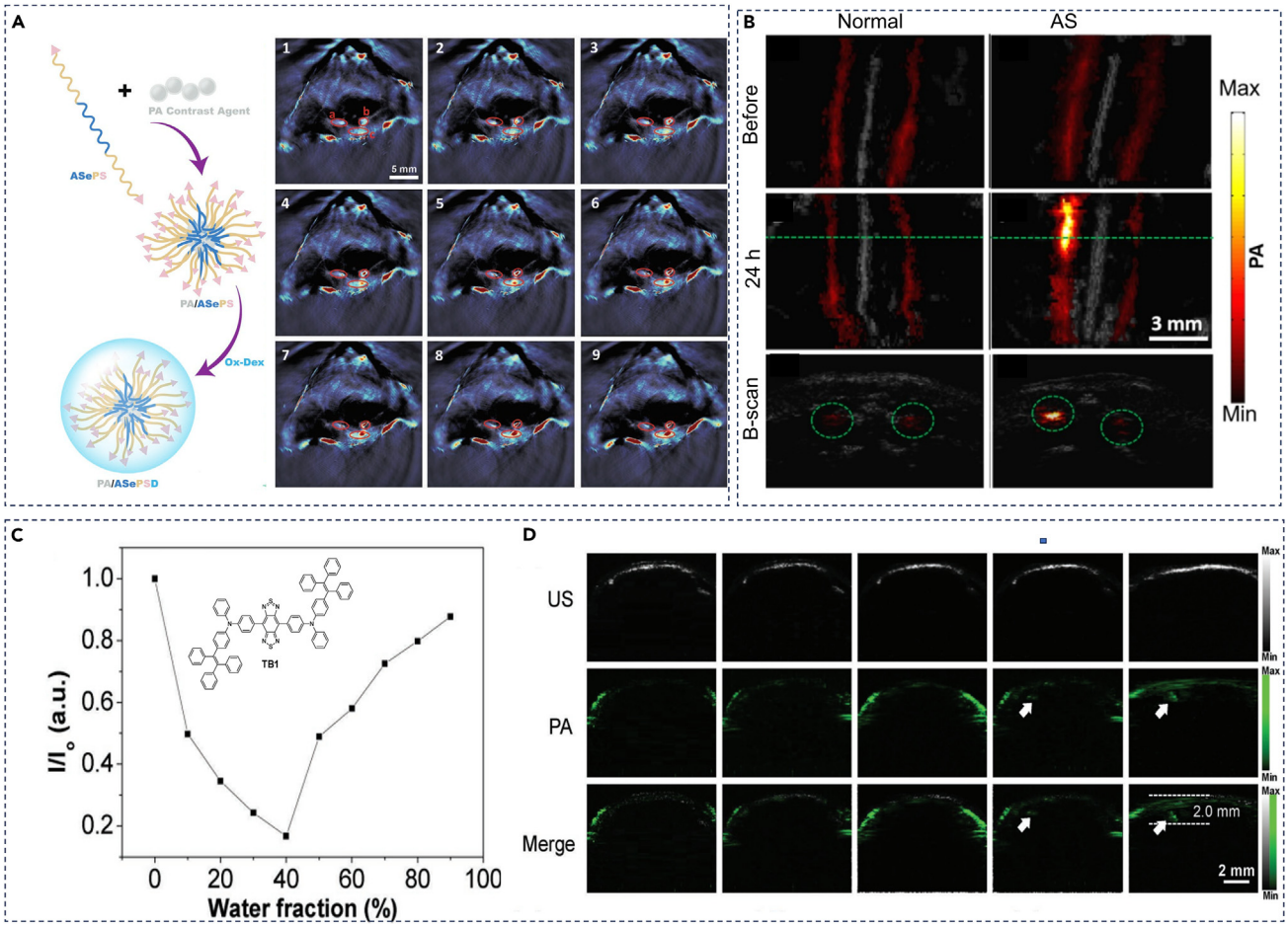

Figure 8. The application of PAI in atherosclerosis imaging

(A) Photoacoustic signal images of different cross-sections among carotid to aortic intervals in ApoE$^{-/-}$ mice. Reproduced with permission from Xu et al.[76] Copyright 2023 WILEY-VCH.

(B) Representative maximum amplitude projection images (PA/ultrasound image) of normal mouse an atherosclerotic mice in pre-treatment, 24 h post PBD-CD36 NPs injection, and B-scan. Reproduced with permission from Xie et al.[77] Copyright 2020 Ivyspring International Publisher.

(C) Chemical structure of TB1 and its AIE characteristic in THF/water mixture with different water fractions.

(D) Noninvasive PAI of orthotopic brain tumor through intact scalp and skull at different time point in TB1-RGD peptide dots-treated group. Reproduced with permission from Sheng et al.[82] Copyright 2018 WILEY-VCH.

PAI capability.[82] In particular, intravascular PAI techniques developed in recent years greatly promotes the clinical application prospect of photoacoustic contrast agents such as AIE.[84,85]

Preclinical study of AIEgens

In order to further verify the clinical application potential of NIR-II imaging AIEgens, researchers conducted NIR-II vascular imaging studies in rats, rabbits, and monkeys. In 2020, Qi et al. employed an NIR-II AIEgen, named BPN-BBT, to delineate brain blood vasculature in rats (Figure 9A). By introducing intramolecular D-A interaction using benzobisthiadiazole (BBT) as an electron acceptor and Bisphenylnaphthalen-1-amine (BPN) as an electron donor, respectively, the maximal absorption of BPN-BBT in the NIR region was found to be above 700 nm, resulting from the long emission range (>1,200 nm) and high brightness of AIEgen, achieving clear visualization with high spatial resolution (~4 μm) and deep penetration (700 μm). This study demonstrated the suitability of NIR-II imaging for small animal models.[86] In 2021, Li et al. used NIR-II AIE nanoparticles for multiscale vascular imaging in rabbits (Figure 9B). Due to the emission maximum beyond 1,000 nm and QY above 10%, these nanoparticles enabled comprehensive and deep intravital vascular fluorescence imaging. This study advances NIR-II imaging to large animals, which subsequently is confirmed by Jiang et al.[87,88] Additionally, Feng et al. utilized a high-efficiency AIEgen with QY of 13.6% in NIR-II window to assess the *in vivo* NIR-II imaging in marmoset (Figure 9C). After intravenous injection of AIEgen, extensive cortical vasculature was captured on an NIR-sensitive camera using a scan lens.[89] The successful imaging in marmoset indicated that the clinical transformation of NIR-II imaging based on AIEgen underscores significant progress.

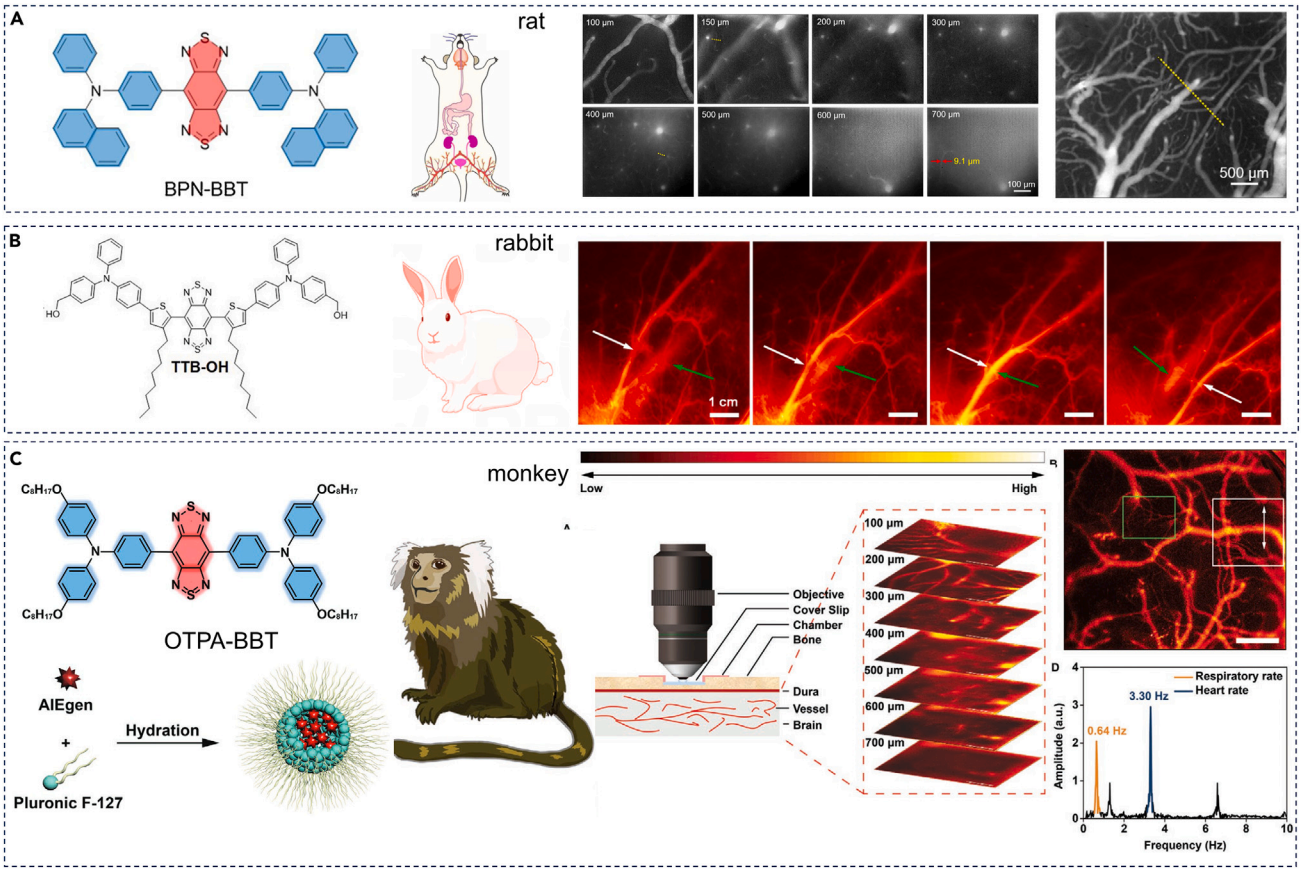

Figure 9. The vessel imaging of AIEgens in different animal models

(A–C) Preclinical trial of AIEgens for the NIR-II imaging of vessel in rat (A), reproduced with permission from Qi et al.[86] Copyright 2020 Elsevier. rabbit (B), Reproduced with permission from Li et al.[90] Copyright 2021 Elsevier. and monkey (C). Reproduced with permission from Feng et al.[89] Copyright 2021 WILEY-VCH.

CONCLUSION AND OUTLOOK

In this mini review, we have showcased the imaging potential of AIEgens including fluorescence imaging, two/multi-photon imaging, and PAI and revealed their applications in angiography and the diagnosis of atherosclerosis. Optical diagnosis is being regarded as one of the next-generation medical diagnostic technologies, owing to its high spatial resolution, rapid data acquisition, absence of radiation risks, cost-effectiveness, minimal invasiveness, and limited side effects. AIEgens, especially the NIR-IIb AIEgens, can provide increased tissue penetration depth with enhanced spatiotemporal resolution and minimal photodamage, making them ideal optical contrast agents.

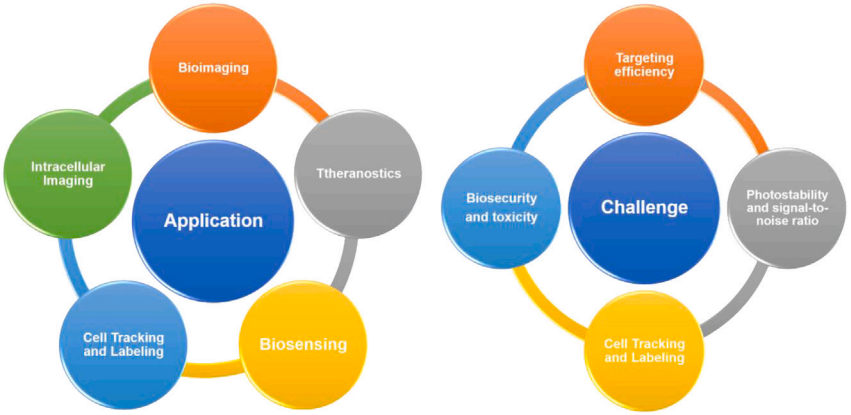

Figure 10. The major application and challenge in the biomedical field

In addition to bioimaging, AIEgens have been applied in the phototherapy of CVD utilizing their photodynamic therapy and photothermal therapy capabilities. When exposed to light, AIEgens can eliminate inflammatory cells at the lesion site by generating ROS or heat, thereby reshaping the microenvironment and facilitating the treatment of CVD. Additionally, AIEgens can also be employed to achieve imaging-guided precision therapy via their excellent imaging performance or be applied in control drug release for CVD therapy. Furthermore, AIEgens are utilized in biosensing for detecting biomolecules and analytes with high sensitivity and specificity, labeling and tracking cells both *in vitro* and *in vivo*, and investigating intracellular processes and organelles by penetrating cell membranes and selectively labeling specific subcellular structure. These capabilities facilitate the visualization of cellular dynamics, organelle morphology, and interactions within living cells, thereby aiding in the comprehension of cellular functions and disease mechanisms.

AIEgens possess numerous advantages and show potential for clinical applications. However, they are still in early stages of development, with several challenges yet to be addressed. To facilitate the clinical application of AIEgens, attention should be given to the following factors. (1) Biosecurity and toxicity: while many AIEgens exhibit low cytotoxicity, comprehensive investigation is necessary to evaluate their potential long-term effects and accumulation in biological systems. Numerous *in vitro* and *in vivo* studies have successfully confirmed that AIEgens exhibit low cytotoxicity, are non-immunogenic, pose minimal risk to blood safety, and do not cause tissue damage when applied *in vivo*. However, the absence of clinical safety studies remains a significant challenge for the clinical application of AIEgens. (2) Targeting efficiency: strategies such as surface functionalization with targeting ligands (e.g., antibodies, peptides) are employed. However, optimizing their binding affinity, specificity, and stability is crucial for effective targeted imaging and therapy. (3) Photostability and signal-to-noise ratio: developing AIEgens with enhanced signal-to-noise ratios and resistance to photobleaching is essential for ensuring reliable and reproducible results in biological samples. (4) Bioavailability and pharmacokinetics: AIEgens must overcome complex biological barriers to effectively reach their intended targets. Improving their bioavailability and pharmacokinetic profiles through appropriate formulation and delivery systems is critical for clinical translation (Figure 10).

In summary, the development of AIEgens has significantly advanced the diagnosis and treatment of major diseases such as cancer, microbial infections, and CVDs like atherosclerosis. Nonetheless, several challenges remain that require further effort to overcome in order to facilitate their clinical translation. With ongoing exploration and development, we expect that AIEgens will make revolutionary discoveries and improve human health by utilizing their diagnosis and treatment performance.

ACKNOWLEDGMENTS

This work was supported by the Shenzhen Science and Technology Program (JCYJ20210324142211031).

DECLARATION OF INTERESTS

The authors declare no competing interests.

REFERENCES

1. Nedkoff, L., Briffa, T., Zemedikun, D., Herrington, S., and Wright, F.L. (2023). Global Trends in Atherosclerotic Cardiovascular Disease. Clin. Therapeut. *45*, 1087–1091.
2. Libby, P., Ridker, P.M., and Hansson, G.K. (2011). Progress and challenges in translating the biology of atherosclerosis. Nature *473*, 317–325.
3. Withers, P.J., Bouman, C., Carmignato, S., Cnudde, V., Grimaldi, D., Hagen, C.K., Maire, E., Manley, M., Du Plessis, A., and Stock, S.R. (2021). X-ray computed tomography. Nat. Rev. Methods Primers *1*, 18.
4. Cooley, C.Z., McDaniel, P.C., Stockmann, J.P., Srinivas, S.A., Cauley, S.F., Śliwiak, M., Sappo, C.R., Vaughn, C.F., Guerin, B., Rosen, M.S., et al. (2021). A portable scanner for magnetic resonance imaging of the brain. Nat. Biomed. Eng. *5*, 229–239.
5. Tarkin, J.M., Joshi, F.R., and Rudd, J.H.F. (2014). PET imaging of inflammation in atherosclerosis. Nat. Rev. Cardiol. *11*, 443–457.
6. Greenwood, J.P., Maredia, N., Younger, J.F., Brown, J.M., Nixon, J., Everett, C.C., Bijsterveld, P., Ridgway, J.P., Radjenovic, A., Dickinson, C.J., et al. (2012). Cardiovascular magnetic resonance and single-photon emission computed tomography for diagnosis of coronary heart disease (CE-MARC): a prospective trial. Lancet *379*, 453–460.
7. Yoon, S., Kim, M., Jang, M., Choi, Y., Choi, W., Kang, S., and Choi, W. (2020). Deep optical imaging within complex scattering media. Nat. Rev. Phys. *2*, 141–158.
8. Ntziachristos, V. (2010). Going deeper than microscopy: the optical imaging frontier in biology. Nat. Methods *7*, 603–614.
9. Altman, R.B., Terry, D.S., Zhou, Z., Zheng, Q., Geggier, P., Kolster, R.A., Zhao, Y., Javitch, J.A., Warren, J.D., and Blanchard, S.C. (2011). Cyanine fluorophore derivatives with enhanced photostability. Nat. Methods *9*, 68–71.
10. Xu, W., Wang, D., and Tang, B.Z. (2021). NIR-II AIEgens: A Win-Win Integration towards Bioapplications. Angew. Chem., Int. Ed. Engl. *60*, 7476–7487.
11. Würthner, F. (2020). Aggregation-Induced Emission (AIE): A Historical Perspective. Angew. Chem. Int. Ed. *59*, 14192–14196.
12. Ding, D., Li, K., Liu, B., and Tang, B.Z. (2013). Bioprobes Based on AIE Fluorogens. Acc. Chem. Res. *46*, 2441–2453.
13. Hu, R., Leung, N.L.C., and Tang, B.Z. (2014). AIE macromolecules: syntheses, structures and functionalities. Chem. Soc. Rev. *43*, 4494–4562.
14. Li, J., Wang, J., Li, H., Song, N., Wang, D., and Tang, B.Z. (2020). Supramolecular materials based on AIE luminogens (AIEgens): construction and applications. Chem. Soc. Rev. *49*, 1144–1172.
15. Alam, P., Leung, N.L., Zhang, J., Kwok, R.T., Lam, J.W., and Tang, B.Z. (2021). AIE-based luminescence probes for metal ion detection. Coord. Chem. Rev. *429*, 213693.
16. Wang, D., and Tang, B.Z. (2019). Aggregation-Induced Emission Luminogens for Activity-Based Sensing. Acc. Chem. Res. *52*, 2559–2570.
17. Sharath Kumar, K.S., Girish, Y.R., Ashrafizadeh, M., Mirzaei, S., Rakesh, K.P., Hossein Gholami, M., Zabolian, A., Hushmandi, K., Orive, G., Kadumudi, F.B., et al. (2021). AIE-featured tetraphenylethylene nanoarchitectures in biomedical application: Bioimaging, drug delivery and disease treatment. Coord. Chem. Rev. *447*, 214135.
18. Wang, S., Liu, J., Goh, C.C., Ng, L.G., and Liu, B. (2019). NIR-II-Excited Intravital Two-Photon Microscopy Distinguishes Deep Cerebral and Tumor Vasculatures with an Ultrabright NIR-I AIE Luminogen. Adv. Mater. *31*, 1904447.
19. Liu, S., Li, Y., Kwok, R.T.K., Lam, J.W.Y., and Tang, B.Z. (2020). Structural and process controls of AIEgens for NIR-II theranostics. Chem. Sci. *12*, 3427–3436.
20. Yan, D., Li, T., Yang, Y., Niu, N., Wang, D., Ge, J., Wang, L., Zhang, R., Wang, D., and Tang, B.Z. (2022). A Water-Soluble AIEgen for Noninvasive Diagnosis of Kidney Fibrosis via SWIR Fluorescence and Photoacoustic Imaging. Adv. Mater. *34*, 2206643.

21. Li, D., Deng, X., Xu, Z., Wang, D., Xu, G., Zhang, P., Qiu, P., Xie, W., Wang, D., Tang, B.Z., and Wang, K. (2023). Molecular Engineering of NIR-II AIE Luminogen Excited at 1700 nm for Ultradeep Intravital Brain Two-Photon Fluorescence Imaging. Adv. Funct. Mater. *33*, 2303967.
22. Teng, R., Yang, Y., Zhang, Z., Yang, K., Sun, M., Li, C., Fan, Z., and Du, J. (2023). In Situ Enzyme-Induced Self-Assembly of Antimicrobial-Antioxidative Peptides to Promote Wound Healing. Adv. Funct. Mater. *33*, 2214454.
23. Ding, Y., Liu, J., Li, X., Xu, L., Li, C., Ma, L., Liu, J., Ma, R., An, Y., Huang, F., et al. (2019). Rational design of drug delivery systems for potential programmable drug release and improved therapeutic effect. Mater. Chem. Front. *3*, 1159–1167.
24. Zheng, C., Zhong, Q., Yi, K., Kong, H., Cao, F., Zhuo, C., Xu, Y., Shi, R., Ju, E., Song, W., et al. (2023). Anti-phagocytosis-blocking repolarization-resistant membrane-fusogenic liposome (ARMFUL) for adoptive cell immunotherapy. Sci. Adv. *9*, eadh2413.
25. Kong, H., Zheng, C., Yi, K., Mintz, R.L., Lao, Y.H., Tao, Y., and Li, M. (2024). An antifouling membrane-fusogenic liposome for effective intracellular delivery *in vivo*. Nat. Commun. *15*, 4267.
26. Zheng, C., Zhong, Q., Song, W., Yi, K., Kong, H., Wang, H., Tao, Y., Li, M., and Chen, X. (2023). Membrane-Fusion-Mediated Multiplex Engineering of Tumor Cell Surface Glycans for Enhanced NK Cell Therapy. Adv. Mater. *35*, 2206989.
27. Li, Y., Hua, L., He, W., Chen, L., Piao, Y., Peng, M., Li, D., Shi, L., and Liu, Y. (2024). Microenvironment-Adaptive Metallo-Polymeric Nanodecoys via Subcomponent Coordination for Bacterial Biofilm Eradication and Immunomodulation. Adv. Funct. Mater. 2405487.
28. Piao, Y.Z., Su, L., Hu, X., He, W., Hu, X., Omolo, C.A., Govender, T., Li, H., Xue, H., Ge, Y., et al. (2024). One-component lipidic bicontinuous nanospheres as a smart drug loading platform to eradicate candida biofilms in oral and vaginal infection. Nano Today *54*, 102123.
29. Qi, J., Hu, X., Dong, X., Lu, Y., Lu, H., Zhao, W., and Wu, W. (2019). Towards more accurate bioimaging of drug nanocarriers: turning aggregation-caused quenching into a useful tool. Adv. Drug Deliv. Rev. *143*, 206–225.
30. Wang, Y.F., Che, J., Zheng, Y.C., Zhao, Y.Y., Chen, F., Jin, S.B., Gong, N.Q., Xu, J., Hu, Z.B., and Liang, X.J. (2015). Multi-stable fluorescent silica nanoparticles obtained from *in situ* doping with aggregation-induced emission molecules. J. Mater. Chem. B *3*, 8775–8781.
31. Xu, L., Jiang, X., Liang, K., Gao, M., and Kong, B. (2022). Frontier luminous strategy of functional silica nanohybrids in sensing and bioimaging: From ACQ to AIE. Aggregate *3*, e121.
32. Cai, Y., Ji, X., Zhang, Y., Liu, C., Zhang, Z., Lv, Y., Dong, X., He, H., Qi, J., Lu, Y., et al. (2023). Near-infrared fluorophores with absolute aggregation-caused quenching and negligible fluorescence re-illumination for *in vivo* bioimaging of nanocarriers. Aggregate *4*, e277.
33. Tsai, W.K., Wang, C.I., Liao, C.H., Yao, C.N., Kuo, T.J., Liu, M.H., Hsu, C.P., Lin, S.Y., Wu, C.Y., Pyle, J.R., et al. (2019). Molecular design of near-infrared fluorescent Pdots for tumor targeting: aggregation-induced emission versus anti-aggregation-caused quenching. Chem. Sci. *10*, 198–207.
34. Feng, H.T., Yuan, Y.X., Xiong, J.B., Zheng, Y.S., and Tang, B.Z. (2018). Macrocycles and cages based on tetraphenylethylene with aggregation-induced emission effect. Chem. Soc. Rev. *47*, 7452–7476.
35. Feng, G., and Liu, B. (2016). Multifunctional AIEgens for Future Theranostics. Small *12*, 6528–6535.
36. Xu, C., Ye, R., Shen, H., Lam, J.W.Y., Zhao, Z., and Zhong Tang, B. (2022). Molecular Motion and Nonradiative Decay: Towards Efficient Photothermal and Photoacoustic Systems. Angew. Chem., Int. Ed. Engl. *61*, e202204604.
37. Wang, H.P., Chen, X., Qi, Y.L., Huang, L.W., Wang, C.X., Ding, D., and Xue, X. (2021). Aggregation-induced emission (AIE)-guided dynamic assembly for disease imaging and therapy. Adv. Drug Deliv. Rev. *179*, 114028.
38. Fan, X., Xia, Q., Zhang, Y., Li, Y., Feng, Z., Zhou, J., Qi, J., Tang, B.Z., Qian, J., and Lin, H. (2021). Aggregation-Induced Emission (AIE) Nanoparticles-Assisted NIR-II Fluorescence Imaging-Guided Diagnosis and Surgery for Inflammatory Bowel Disease (IBD). Adv. Healthcare Mater. *10*, 2101043.
39. Feng, G., and Liu, B. (2018). Aggregation-Induced Emission (AIE) Dots: Emerging Theranostic Nanolights. Acc. Chem. Res. *51*, 1404–1414.
40. Liu, J., He, Z., Zhong, Y., Zhu, L., Yan, M., Mou, N., Qu, K., Qin, X., Wang, G., Zhang, K., et al. (2023). Reactive Oxygen Species-Responsive Sequentially Targeted AIE Fluorescent Probe for Precisely Identifying the Atherosclerotic Plaques. ACS Appl. Mater. Interfaces *15*, 47381–47393.
41. Ma, B., Xu, H., Wang, Y., Yang, L., Zhuang, W., Li, G., and Wang, Y. (2021). Biomimetic-Coated Nanoplatform with Lipid-Specific Imaging and ROS Responsiveness for Atherosclerosis-Targeted Theranostics. ACS Appl. Mater. Interfaces *13*, 35410–35421.
42. Zhang, Y., Zhuang, W., Chen, J., Li, C., Li, S., and Chen, M. (2023). Aggregation-induced emission fluorescent probes for lipid droplets-specific bioimaging of cells and atherosclerosis plaques. Spectrochim. Acta Mol. Biomol. Spectrosc. *286*, 122017.
43. He, Z., Chen, Q., Duan, X., Zhong, Y., Zhu, L., Mou, N., Yang, X., Cao, Y., Han, Z., He, H., et al. (2024). Reactive oxygen species-responsive nano-platform with dual-targeting and fluorescent lipid-specific imaging capabilities for the management of atherosclerotic plaques. Acta Biomater. *181*, 375–390.
44. Ma, D., Zhuang, W., Liu, Q., Chen, J., Li, C., Li, S., and Chen, M. (2023). A pH-responsive nanoplatform with aggregation-induced emission features for lipid droplet imaging in atherosclerosis. Chem. Eng. J. *476*, 146792.
45. Guo, B., Sheng, Z., Hu, D., Liu, C., Zheng, H., and Liu, B. (2018). Through Scalp and Skull NIR-II Photothermal Therapy of Deep Orthotopic Brain Tumors with Precise Photoacoustic Imaging Guidance. Adv. Mater. *30*, 1802591.
46. Kenry, Duan, Y., and Liu, B. (2018). Recent Advances of Optical Imaging in the Second Near-Infrared Window. Adv. Mater. *30*, 1802394.
47. Li, J., Liu, Y., Xu, Y., Li, L., Sun, Y., and Huang, W. (2020). Recent advances in the development of NIR-II organic emitters for biomedicine. Coord. Chem. Rev. *415*, 213318.
48. Liu, S., Chen, C., Li, Y., Zhang, H., Liu, J., Wang, R., Wong, S.T.H., Lam, J.W.Y., Ding, D., and Tang, B.Z. (2020). Constitutional Isomerization Enables Bright NIR-II AIEgen for Brain-Inflammation Imaging. Adv. Funct. Mater. *30*, 1908125.
49. Qu, C., Xiao, Y., Zhou, H., Ding, B., Li, A., Lin, J., Zeng, X., Chen, H., Qian, K., Zhang, X., et al. (2019). Quaternary Ammonium Salt Based NIR-II Probes for In Vivo Imaging. Adv. Opt. Mater. *7*, 1900229.
50. Qin, Y., Li, X., Lu, S., Kang, M., Zhang, Z., Gui, Y., Li, X., Wang, D., and Tang, B.Z. (2023). Modular Construction of AIE-Active Supramolecular Cages with Tunable Fluorescence for NIR-II Blood Vessel Imaging. ACS Mater. Lett. *5*, 1982–1991.
51. Xu, P., Kang, F., Yang, W., Zhang, M., Dang, R., Jiang, P., and Wang, J. (2020). Molecular engineering of a high quantum yield NIR-II molecular fluorophore with aggregation-induced emission (AIE) characteristics for *in vivo* imaging. Nanoscale *12*, 5084–5090.
52. Gao, D., Li, Y., Wu, Y., Liu, Y., Hu, D., Liang, S., Liao, J., Pan, M., Zhang, P., Li, K., et al. (2023). Albumin-Consolidated AIEgens for Boosting Glioma and Cerebrovascular NIR-II Fluorescence Imaging. ACS Appl. Mater. Interfaces *15*, 3–13.
53. Meng, J., Feng, Z., Qian, S., Wang, C., Li, X., Gao, L., Ding, Z., Qian, J., and Liu, Z. (2022). Mapping physiological and pathological functions of cortical vasculature through aggregation-induced emission nanoprobes assisted quantitative, *in vivo* NIR-II imaging. Biomater. Adv. *136*, 212760.
54. Li, Y., Zhu, H., Wang, X., Cui, Y., Gu, L., Hou, X., Guan, M., Wu, J., Xiao, Y., Xiong, X., et al. (2022). Small-Molecule Fluorophores for Near-Infrared IIb Imaging and Image-Guided Therapy of Vascular Diseases. CCS Chem. *4*, 3735–3750.
55. Li, Y., Cai, Z., Liu, S., Zhang, H., Wong, S.T.H., Lam, J.W.Y., Kwok, R.T.K., Qian, J., and Tang, B.Z. (2020). Design of AIEgens for near-infrared IIb imaging through structural modulation at molecular and morphological levels. Nat. Commun. *11*, 1255.
56. Li, Q., Ding, Q., Li, Y., Zeng, X., Liu, Y., Lu, S., Zhou, H., Wang, X., Wu, J., Meng, X., et al. (2020). Novel small-molecule fluorophores for *in vivo* NIR-IIa and NIR-IIb imaging. Chem. Commun. *56*, 3289–3292.
57. Liu, Y., Li, Y., Koo, S., Sun, Y., Liu, Y., Liu, X., Pan, Y., Zhang, Z., Du, M., Lu, S., et al. (2022). Versatile Types of Inorganic/Organic NIR-IIa/IIb Fluorophores: From Strategic Design toward Molecular Imaging and Theranostics. Chem. Rev. *122*, 209–268.
58. Oheim, M., Michael, D.J., Geisbauer, M., Madsen, D., and Chow, R.H. (2006). Principles of two-photon excitation fluorescence microscopy and other nonlinear imaging approaches. Adv. Drug Deliv. Rev. *58*, 788–808.
59. Helmchen, F., and Denk, W. (2005). Deep tissue two-photon microscopy. Nat. Methods *2*, 932–940.
60. Cahalan, M.D., Parker, I., Wei, S.H., and Miller, M.J. (2002). Two-photon tissue imaging: seeing the immune system in a fresh light. Nat. Rev. Immunol. *2*, 872–880.
61. Zong, W., Wu, R., Li, M., Hu, Y., Li, Y., Li, J., Rong, H., Wu, H., Xu, Y., Lu, Y., et al. (2017). Fast high-resolution miniature two-photon microscopy for brain imaging in freely behaving mice. Nat. Methods *14*, 713–719.
62. Mahou, P., Vermot, J., Beaurepaire, E., and Supatto, W. (2014). Multicolor two-photon light-sheet microscopy. Nat. Methods *11*, 600–601.

63. Samanta, S., Huang, M., Li, S., Yang, Z., He, Y., Gu, Z., Zhang, J., Zhang, D., Liu, L., and Qu, J. (2021). AIE-active two-photon fluorescent nanoprobe with NIR-II light excitability for highly efficient deep brain vasculature imaging. Theranostics *11*, 2137–2148.
64. Situ, B., Gao, M., He, X., Li, S., He, B., Guo, F., Kang, C., Liu, S., Yang, L., Jiang, M., et al. (2019). A two-photon AIEgen for simultaneous dual-color imaging of atherosclerotic plaques. Mater. Horiz. *6*, 546–553.
65. Ma, B., Xu, H., Zhuang, W., Wang, Y., Li, G., and Wang, Y. (2020). Reactive Oxygen Species Responsive Theranostic Nanoplatform for Two-Photon Aggregation-Induced Emission Imaging and Therapy of Acute and Chronic Inflammation. ACS Nano *14*, 5862–5873.
66. Horton, N.G., Wang, K., Kobat, D., Clark, C.G., Wise, F.W., Schaffer, C.B., and Xu, C. (2013). In vivo three-photon microscopy of subcortical structures within an intact mouse brain. Nat. Photonics *7*, 205–209.
67. Wang, T., Ouzounov, D.G., Wu, C., Horton, N.G., Zhang, B., Wu, C.H., Zhang, Y., Schnitzer, M.J., and Xu, C. (2018). Three-photon imaging of mouse brain structure and function through the intact skull. Nat. Methods *15*, 789–792.
68. Xu, Z., Zhang, Z., Deng, X., Li, J., Jiang, Y., Law, W.C., Yang, C., Zhang, W., Chen, X., Wang, K., et al. (2022). Deep-Brain Three-Photon Imaging Enabled by Aggregation-Induced Emission Luminogens with Near-Infrared-III Excitation. ACS Nano *16*, 6712–6724.
69. Li, J., Zhang, Z., Deng, X., Xu, Z., Wang, L., Xu, G., Wang, K., Wang, D., and Tang, B.Z. (2022). A potent luminogen with NIR-IIb excitable AIE features for ultradeep brain vascular and hemodynamic three-photon imaging. Biomaterials *287*, 121612.
70. Wang, S., Li, X., Chong, S.Y., Wang, X., Chen, H., Chen, C., Ng, L.G., Wang, J.W., and Liu, B. (2021). In Vivo Three-Photon Imaging of Lipids using Ultrabright Fluorogens with Aggregation-Induced Emission. Adv. Mater. *33*, 2007490.
71. Zhu, Z., Leung, C.W.T., Zhao, X., Wang, Y., Qian, J., Tang, B.Z., and He, S. (2015). Using AIE Luminogen for Long-term and Low-background Three-Photon Microscopic Functional Bioimaging. Sci. Rep. *5*, 15189.
72. Qin, W., Alifu, N., Lam, J.W.Y., Cui, Y., Su, H., Liang, G., Qian, J., and Tang, B.Z. (2020). Facile Synthesis of Efficient Luminogens with AIE Features for Three-Photon Fluorescence Imaging of the Brain through the Intact Skull. Adv. Mater. *32*, 2000364.
73. Lin, L., and Wang, L.V. (2022). The emerging role of photoacoustic imaging in clinical oncology. Nat. Rev. Clin. Oncol. *19*, 365–384.
74. Weber, J., Beard, P.C., and Bohndiek, S.E. (2016). Contrast agents for molecular photoacoustic imaging. Nat. Methods *13*, 639–650.
75. Zhang, H.F., Maslov, K., Stoica, G., and Wang, L.V. (2006). Functional photoacoustic microscopy for high-resolution and noninvasive *in vivo* imaging. Nat. Biotechnol. *24*, 848–851.
76. Xu, H., She, P., Zhao, Z., Ma, B., Li, G., and Wang, Y. (2023). Duplex Responsive Nanoplatform with Cascade Targeting for Atherosclerosis Photoacoustic Diagnosis and Multichannel Combination Therapy. Adv. Mater. *35*, 2300439.
77. Xie, Z., Yang, Y., He, Y., Shu, C., Chen, D., Zhang, J., Chen, J., Liu, C., Sheng, Z., Liu, H., et al. (2020). In vivo assessment of inflammation in carotid atherosclerosis by noninvasive photoacoustic imaging. Theranostics *10*, 4694–4704.
78. Ma, B., Xiao, Y., Lv, Q., Li, G., Wang, Y., and Fu, G. (2023). Targeting Theranostics of Atherosclerosis by Dual-Responsive Nanoplatform via Photoacoustic Imaging and Three-In-One Integrated Lipid Management. Adv. Mater. *35*, 2206129.
79. Ge, X., Cui, H., Kong, J., Lu, S.Y., Zhan, R., Gao, J., Xu, Y., Lin, S., Meng, K., Zu, L., et al. (2020). A Non-Invasive Nanoprobe for In Vivo Photoacoustic Imaging of Vulnerable Atherosclerotic Plaque. Adv. Mater. *32*, 2000037.
80. Gifani, M., Eddins, D.J., Kosuge, H., Zhang, Y., Paluri, S.L.A., Larson, T., Leeper, N., Herzenberg, L.A., Gambhir, S.S., McConnell, M.V., et al. (2021). Ultraselective Carbon Nanotubes for Photoacoustic Imaging of Inflamed Atherosclerotic Plaques. Adv. Funct. Mater. *31*, 2101005.
81. Qin, H., Zhao, Y., Zhang, J., Pan, X., Yang, S., and Xing, D. (2016). Inflammation-targeted gold nanorods for intravascular photoacoustic imaging detection of matrix metalloproteinase-2 (MMP2) in atherosclerotic plaques. Nanomedicine *12*, 1765–1774.
82. Sheng, Z., Guo, B., Hu, D., Xu, S., Wu, W., Liew, W.H., Yao, K., Jiang, J., Liu, C., Zheng, H., and Liu, B. (2018). Bright Aggregation-Induced-Emission Dots for Targeted Synergetic NIR-II Fluorescence and NIR-I Photoacoustic Imaging of Orthotopic Brain Tumors. Adv. Mater. *30*, 1800766.
83. Li, P., He, X., Li, Y., Lam, J.W.Y., Kwok, R.T.K., Wang, C.C., Xia, L.G., and Tang, B.Z. (2022). Recent advances in aggregation-induced emission luminogens in photoacoustic imaging. Eur. J. Nucl. Med. Mol. Imag. *49*, 2560–2583.
84. Jansen, K., van der Steen, A.F.W., van Beusekom, H.M.M., Oosterhuis, J.W., and van Soest, G. (2011). Intravascular photoacoustic imaging of human coronary atherosclerosis. Opt. Lett. *36*, 597–599.
85. Wang, B., Su, J.L., Karpiouk, A.B., Sokolov, K.V., Smalling, R.W., and Emelianov, S.Y. (2010). Intravascular Photoacoustic Imaging. IEEE J. Quant. Electron. *16*, 588–599.
86. Qi, J., Alifu, N., Zebibula, A., Wei, P., Lam, J.W., Peng, H.Q., Kwok, R.T., Qian, J., and Tang, B.Z. (2020). Highly stable and bright AIE dots for NIR-II deciphering of living rats. Nano Today *34*, 100893.
87. Jiang, Z.Z., Geng, X.R., Su, L.L., Chen, A.N., Sheng, Z.H., and Jiang, T.A. (2022). Neutrophil membrane camouflaged nanoprobes for NIR-II fluorescence imaging of inflamed, high-risk atherosclerotic plaques in mouse and rabbit models. Mater. Today Chem. *26*, 101062.
88. Tian, C., Xue, X., Chen, Y., Liu, R., Wang, Y., Ye, S., Fu, Z., Luo, Y., Wang, S., He, X., and Pang, H. (2022). Phosphotungstate Acid Doped Polyanilines Nanorods for *in situ* NIR-II Photothermal Therapy of Orthotopic Hepatocellular Carcinoma in Rabbit. Int. J. Nanomed. *17*, 5565–5579.
89. Feng, Z., Bai, S., Qi, J., Sun, C., Zhang, Y., Yu, X., Ni, H., Wu, D., Fan, X., Xue, D., et al. (2021). Biologically Excretable Aggregation-Induced Emission Dots for Visualizing Through the Marmosets Intravitally: Horizons in Future Clinical. Adv. Mater. *33*, 2008123.
90. Li, Y., Hu, D., Sheng, Z., Min, T., Zha, M., Ni, J.S., Zheng, H., and Li, K. (2021). Self-assembled AIEgen nanoparticles for multiscale NIR-II vascular imaging. Biomaterials *264*, 120365.